Comput Mech (2010) 46:867–881
DOI 10.1007/s00466-010-0516-y

ORIGINAL PAPER

Dispersion free analysis of acoustic problems using the alpha finite element method

Z. C. He · G. R. Liu · Z. H. Zhong · G. Y. Zhang · A. G. Cheng

Received: 4 May 2010 / Accepted: 4 July 2010 / Published online: 28 July 2010

Abstract The classical finite element method (FEM) fails to provide accurate results to the Helmholtz equation with large wave numbers due to the well-known "pollution error" caused by the numerical dispersion, i.e. the numerical wave number is always smaller than the exact one. This dispersion error is essentially rooted at the "overly-stiff" feature of the FEM model. In this paper, an alpha finite element method (α-FEM) is then formulated for the acoustic problems by combining the "smaller wave number" model of FEM and the "larger wave number" model of NS-FEM through a scaling factor $a \in [0, 1]$. The motivation for this combined approach is essentially from the features of "overly-stiff" FEM model and "overly-soft" NS-FEM model, and accurate solutions can be obtained by tuning the α-FEM model. A technique is proposed to determine a particular alpha with which the α-FEM model can possess a very "close-to-exact" stiffness, which can effectively reduce the dispersion error leading to dispersion free solutions for acoustic problems. Theoretical and numerical studies shall demonstrate the excellent properties of the present α-FEM.

Z. C. He (✉) · Z. H. Zhong · A. G. Cheng
State Key Laboratory of Advanced Design and Manufacturing for Vehicle Body, Hunan University, 410082 Changsha, People's Republic of China
e-mail: hezhicheng815@gmail.com

Z. C. He · G. R. Liu
Department of Mechanical Engineering, Centre for Advanced Computations in Engineering Science (ACES), National University of Singapore, 9 Engineering Drive 1, Singapore 117576, Singapore

G. R. Liu · G. Y. Zhang
Singapore-MIT Alliance (SMA), E4-04-10, 4 Engineering Drive 3, Singapore 117576, Singapore

Keywords Numerical method · Meshfree method · Finite element method (FEM) · Alpha finite element method (α-FEM) · Acoustic · Numerical error

1 Introduction

As the increasing concerns on the acoustic performance of enclosed cavities, such as the aircraft cabins and automobile passenger compartments, careful considerations are required in designing such sophisticated structures. Therefore, numerical methods for solving acoustic problems governed by the Helmholtz equation are becoming more and more important. The standard finite element method (FEM) has been established and widely-used in solving general structural-acoustic problems. However, it is known that the FEM can only provide reliable predictions in the low frequency range, and much effort is currently spent in improving quality of the FEM solution in high frequency range. Within the standard framework of Galerkin weak formulations, such efforts have fundamental difficulties. This is because the Helmholtz operator may lose the ellipticity with increasing wave number [1], leading to the well-known "pollution error".

Studies have found that the pollution error for one-dimensional problems can be avoided, while for two (and higher) dimensional problems no such methods are pollution free [2], and various numerical methods have been proposed. They are, (i) the stabilized FEM, such as the Galerkin/least-squares finite element method (GLS) [3,4], the quasi-stabilized finite element method (QSFEM) [5]. (ii) higher order methods, such as generalized high order approximations (p-version) [6,7], the partition of unity method (PUM) [8,9] and the discontinuous enrichment method (DEM) [10,11] (iii) meshless method, such as element-free Galerkin method (EFGM) [12,13]. They all can give improved

solutions compared to the standard FEM, however, properly "softened" stiffness for the discrete model is much more effective and direct to the root of the numerical pollution error [14].

Due to the fact that the discretized model based on the standard Galerkin weak form behaviors stiffer than the continuous system [15], and the speed of sound propagating in the overly-stiff discretized model is higher than the real speed of sound. This also means that the wave number in the FEM model is smaller than the actual one, leading to the so-called numerical dispersive error. In order to soften the discretized system, a formulation of generalized smoothed Galerkin weak form [16] has been proposed for general meshfree settings [17], allowing the use of both continuous and discontinuous field functions and both compatible and incompatible strain fields. For the FEM settings, smoothed finite element methods (S-FEM) have also been systematically formulated [15]. Using the node-based strain smoothing technique, a node-based smoothed point interpolation method (NS-PIM or LC-PIM) [18,19] and node-based finite element method (NS-FEM) [20] have been formulated. It has been found the NS-PIM and NS-FEM can provide upper bound solution to the exact one in energy norm for elasticity problems with homogeneous essential boundary conditions [20,21]. This property implies that the NS-PIM and NS-FEM model are softer than the exact model. However, the NS-PIM and NS-FEM models behave "overly-soft" leading to the so-called temporal instability observed as spurious non-zero energy modes in vibration analysis [22]. An alpha finite element method (α-FEM) was then proposed [23] by combining the "over-stiffness" of the FEM and the "over-softness" of the NS-FEM through a parameter α, resulting in a numerical model with very close-to-exact stiffness. This idea is very useful in developing "ultra-accurate" numerical models. However, the parameter α was found depending on the problems and mesh used, thus the alpha is inconvenient to determine for different problems or problems with different mesh.

In this work, the characteristic of NS-FEM for acoustic problems is firstly theoretical addressed, and the wave number of NS-FEM is found to be always larger than the exact one, which is essentially caused by the "overly-soft" model. By introducing a scaled factor $\alpha \in [0, 1]$, the α-FEM which makes the best use of the "overly-stiff" of FEM and the "overly-soft" of NS-FEM is then formulated for 1D and 2D acoustic problems. The parameter alpha which controls the contributions from both the standard FEM and the NS-FEM can be determined by the tuned model. With so-determined α, the α-FEM can produce a very "close-to-exact" stiffness to the discretized system, thus the error in the α-FEM is only an interpolation error and is free of dispersion. In 1D problems, the parameter α depends on the wave number and mesh size, while in 2D problems, the direction of wave propagation is another factor which determines the parameter α, so the optimal parameter alpha is obtained to remedy this difficulty which reduces phase error for all possible wave vector directions.

The paper is organized as follows: Section 2 briefly describes the mathematical model of the acoustic problems. Section 3 introduces the detailed formulation of alpha finite element method for acoustic problems. Section 4 outlines the issue of the numerical error. In Sect. 5, the determination of alpha for 1D and 2D problems are presented. Numerical examples are studied in detail in Sect. 6. Finally, the conclusions from the numerical results are made in Sect. 7.

2 Mathematical model of acoustic problems

Consider an acoustic problem domain Ω with boundary Γ decomposed into three portions Γ_D, Γ_N and Γ_A, which $\Gamma = \Gamma_D \cup \Gamma_N \cup \Gamma_A$. The Dirichlet, Neumann and admittance (Robin) boundary conditions are prescribed on Γ_D, Γ_N and Γ_A, respectively. Let p' denote the acoustic field pressure and c be the speed of sound traveling in the fluid. The acoustic wave equation can be written in the following standard form:

$$\nabla^2 p' - \frac{1}{c^2}\frac{\partial^2 p'}{\partial t^2} = 0 \tag{1}$$

where ∇^2 and t denote the Laplace operator and time, respectively. Here we assume that the acoustic pressure p' is a small harmonic perturbation around a steady state in the fluid. The acoustic pressure can be expressed as:

$$p' = pe^{j\omega t} \tag{2}$$

where $j = \sqrt{-1}$, ω is the angular frequency and the p is the amplitude of the acoustic wave. In general, the acoustic pressure p is complex-valued in the frequency domain, and satisfies the Helmholtz equation given by:

$$\nabla^2 p + k^2 p = 0 \tag{3}$$

where k is the wave number defined by

$$k = \frac{\omega}{c} \tag{4}$$

Because the acoustic particle velocity v in an ideal fluid is proportional to the gradient of acoustic pressure, we shall have:

$$\nabla p + j\rho\omega v = 0 \tag{5}$$

For interior acoustic problems, three types of boundary conditions containing the Dirichlet, Neumann and admittance (Robin) boundary conditions on Γ_D, Γ_N and Γ_A can be described as follows:

$$p = p_D \quad \text{on } \Gamma_D \tag{6}$$

$$\nabla p \cdot n = -j\rho\omega v_n \quad \text{on } \Gamma_N \tag{7}$$

$$\nabla p \cdot n = -j\rho\omega A_n p \quad \text{on } \Gamma_A \tag{8}$$

where v_n, ρ and A_n represent the normal velocity on the boundary Γ_N, the density of medium and the admittance coefficient on boundary Γ_A, respectively.

A weak form of Helmholtz equation is obtained by multiplying Eq. (3) with a test function w, integrating the product over the entire domain, using integration by part and applying the boundary conditions shown in Eqs. (6)–(8), the weak form of the acoustic problem can then be expressed as follows

$$-\int_\Omega \nabla w \cdot \nabla p \mathrm{d}\Omega + k^2 \int_\Omega wp\mathrm{d}\Omega - j\rho\omega \int_{\Gamma_N} wv_n \mathrm{d}\Gamma - j\rho\omega A_n \int_{\Gamma_A} wp\mathrm{d}\Gamma = 0 \tag{9}$$

Comparing with Eq. (3) that contains 2nd derivatives, Eq. (9) contains only the first derivatives: the consistence requirement of Eq. (9) on the field functions is weaker.

3 Formulation of the α-FEM

3.1 Briefing on the finite element method

In the standard FEM, the field variable pressure p can be expressed in the approximate form:

$$p = \sum_{i=1}^{m} N_i p_i = \mathbf{NP} \tag{10}$$

where N_i is the nodal shape function for node i obtained using standard finite element procedure and p_i is the unknown nodal pressure. In standard Galerkin weak form the shape function $\mathbf{N}$ is also used as the weight function w and the weak form for acoustic problems can be obtained as:

$$-\int_\Omega (\nabla \mathbf{N})^{\mathrm{T}} \nabla \mathbf{N}\mathbf{P}\mathrm{d}\Omega - k^2 \int_\Omega \mathbf{N}^{\mathrm{T}}\mathbf{N}\mathbf{P}\mathrm{d}\Omega + j\rho\omega \int_{\Gamma_N} \mathbf{N}^{\mathrm{T}} v_n \mathrm{d}\Gamma + j\rho\omega \int_{\Gamma_A} \mathbf{N}^{\mathrm{T}}\mathbf{N}A_n\mathbf{P}\mathrm{d}\Gamma = 0 \tag{11}$$

which contains only the first derivations of nodal shape functions. The discretized system equations can be finally obtained and written in the following matrix form:

$$[\mathbf{K}^{\mathrm{FEM}} - k^2\mathbf{M} + j\rho\omega\mathbf{C}]\{\mathbf{P}\} = -j\rho\omega\{\mathbf{F}\} \tag{12}$$

where

$$\mathbf{K}^{\mathrm{FEM}} = \int_\Omega (\nabla \mathbf{N})^{\mathrm{T}} (\nabla \mathbf{N})\, \mathrm{d}\Omega$$

The acoustic stiffness matrix (13)

$$\mathrm{M}^{\mathrm{FEM}} = \int_\Omega \mathbf{N}^{\mathrm{T}}\mathbf{N}\mathrm{d}\Omega$$

The acoustic mass matrix (14)

$$\mathbf{C} = \int_{\Gamma_A} \mathbf{N}^{\mathrm{T}}\mathbf{N}A_n\mathrm{d}\Gamma$$

The acoustic damping matrix (15)

$$\mathbf{F} = \int_{\Gamma_N} \mathbf{N}^{\mathrm{T}} v_n \mathrm{d}\Gamma$$

The vector of nodal acoustic forces (16)

$$\{\mathbf{P}\}^{\mathrm{T}} = \{p_1, p_2, \ldots, p_n\}$$

Nodal acoustic pressure in the domain (17)

3.2 Briefing on the node-based smoothed finite element method

In the scheme of NS-FEM, the problem domain is first divided into N_e elements with a total of N_n nodes. The generated cells are exactly the same as those used in the FEM and are used as background cells in the NS-FEM. On top of the background cells, the problem domain is further divided into N_n node-based smoothing domains following the "no-sharing" rule [16], such that $\boxed{\Omega} = \cup_{k=1}^{N_n} \boxed{\Omega}_k$ and $\Omega_k \cap \Omega_l = 0, \forall k \neq l$. For 1D problems, as shown in Fig. 1a, for the interior node k, the smoothing domain Ω_k is formed by connecting two midpoints of elements $k-1$ and k; while for boundary node, the smoothing domain is constructed by connecting this node and the midpoint of the host element. Extending the smoothing domain Ω_k for 2D problems as shown in Fig. 1b, the smoothing domain Ω_k is created by connecting sequentially the mid-edge-point to the centroids of the surrounding triangles of node k. The boundary of the smoothing domain Ω_k is labeled as Γ_k and the union of all Ω_k forms exactly the global domain Ω.

In the NS-FEM, the field variable is constructed using the linear FEM shape functions, which can be created in the same way as those in the FEM, while the difference is that the compatible gradient component $\nabla\mathbf{N}$ is replaced by the smoothed item $\overline{\nabla\mathbf{N}}$ obtained using the node-based gradient smoothing operation [18–20], and the global smoothed acoustic stiffness matrix of NS-FEM can be written as:

$$\overline{\mathbf{K}}^{\mathrm{NS-FEM}} = \int_\Omega \left(\overline{\nabla\mathbf{N}}\right)^{\mathrm{T}} \left(\overline{\nabla\mathbf{N}}\right) \mathrm{d}\Omega$$

The smoothed acoustic stiffness matrix (18)

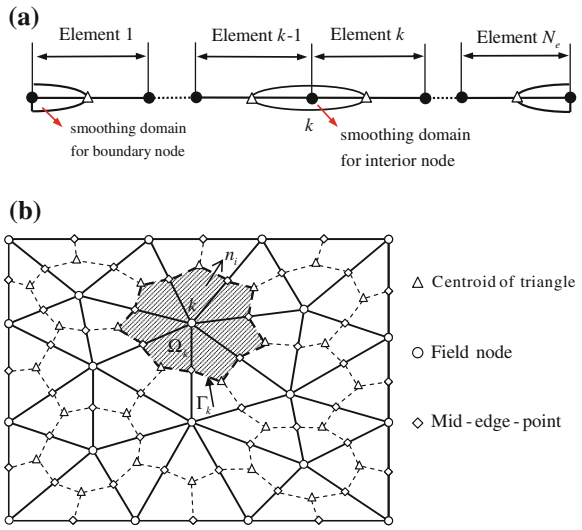

Fig. 1 Node-based smoothing domains and the background mesh. **a** Background mesh and node-based smoothing domain for 1D domain. **b** Background triangular cells and node-based smoothing domains for node k for 2D domain

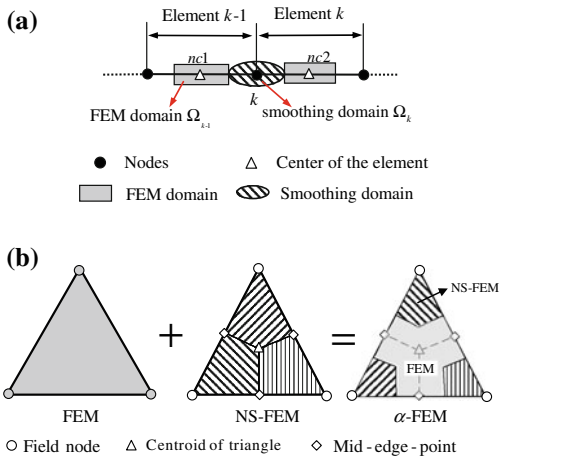

Fig. 2 Illustration of domain discretization for α-FEM. **a** The illustration of α-FEM for 1D problem. **b** The α-FEM for 2D problem is formulated by combining of the FEM and NS-FEM: the NS-FEM is used for three quadrilateral smoothing domains and FEM is used for the Y-shaped area

The above integration is evaluated based on the summation of all the node-based smoothing domains as:

$$\overline{\mathbf{K}}^{\mathrm{NS-FEM}} = \sum_{k=1}^{N_n} \overline{\mathbf{K}}^{(k)} \tag{19}$$

where the $\overline{\mathbf{K}}^{(k)}$ is the local smoothed stiffness matrix associated with node k, and can be calculated:

$$\overline{\mathbf{K}}^{(k)} = \int_{\Omega_k} \overline{\mathbf{B}}^T \overline{\mathbf{B}} \mathrm{d}\Omega = \overline{\mathbf{B}}^{\mathrm{T}} \overline{\mathbf{B}} A_k \tag{20}$$

where $A_k = \int_{\Omega_k} \mathrm{d}\Omega$ is the length (area) of smoothing domain for node k in 1D (2D) problems, and

$$\overline{\mathbf{B}}_i^T(\mathbf{x}_k) = \left[\overline{b}_{i1}\right] \quad (\text{for 1D problem}) \tag{21}$$

$$\overline{\mathbf{B}}_i(\mathbf{x}_k) = \frac{1}{A_k} \int_{\Gamma_k} N_i(\mathbf{x}) n_p(\mathbf{x}) \mathrm{d}\Gamma \tag{22}$$

$$\overline{\mathbf{B}}_i^T(\mathbf{x}_k) = [\,\overline{b}_{i1}\ \overline{b}_{i2}\,] \quad (\text{for 2D problem}) \tag{23}$$

$$\overline{b}_{ip} = \frac{1}{A_k} \int_{\Gamma_k} N_i(\mathbf{x}) n_p(\mathbf{x}) \mathrm{d}\Gamma \tag{24}$$

where N_i is the FEM shape function for node i. Note that in computing $\overline{\mathbf{K}}^{(k)}$ for NS-FEM, we use Eqs. (22) and (24) where only the shape functions (not the derivatives of the shape functions) are used. This implies that the requirement on the nodal shape function is further weakened compared to the standard Galerkin weak form. Therefore, it is termed as weakened weak (W^2) formulation [17,24–27].

3.3 The combination of the FEM and NS-FEM

The α-FEM [23] combines the NS-FEM and the standard FEM by introducing a scaled factor $a \in [0, 1]$. For 1D problem, the NS-FEM divides each element into two equal parts and each part is used to make the contribution to the local stiffness matrix of the node-based domain. In the α-FEM, as shown in Fig. 2a, each element is divided into three parts, i.e. two smoothing domains scaled down by α with equal length of $\frac{1}{2}\alpha h$ (h is the element size) and one FEM domain with a length of $(1-\alpha)\,h$. In the smoothing domains and FEM domains, the NS-FEM and FEM formulations are constructed respectively. For one particular triangular element in 2D domain, the NS-FEM divides the triangle into three quadrilaterals of equal area and each quadrilateral makes the contribution to the local stiffness matrix of the node attached to the quadrilateral, as shown in the second figure of Fig. 2b. In the α-FEM, as shown in Fig. 2b, each triangular element is divided into four parts with a scaled factor α: three quadrilaterals associated with three vertexes with equal area of $\frac{1}{3}\alpha A_{\mathrm{e}}$ and the remaining Y-shaped part in the middle of the element with a area of $(1-\alpha)A_e$, where the A_e is the area of the triangular element. The NS-FEM and the FEM formulations are constructed respectively in the three quadrilaterals and the Y-shaped area for each element.

The entries in sub-matrices of the system stiffness matrix $\mathrm{K}^{\alpha-FEM}$ will be the assembly from the entries of both the NS-FEM and the FEM, and has the following form

$$\mathbf{K}_{IJ}^{\alpha-\mathrm{FEM}} = \sum_{m=1}^{N^e} \mathbf{K}_{IJ(m)}^{\mathrm{FEM}} + \alpha \sum_{n=1}^{N^n} \overline{\mathbf{K}}_{IJ(n)}^{\mathrm{NS-FEM}} \tag{25}$$

where N^e and N^n are the numbers of total elements and total nodes in the entire problem domain, respectively. The stiffness matrix $\mathbf{K}^{\mathrm{FEM}}$ and $\mathbf{K}^{\mathrm{NS-FEM}}$ can be calculated by Eqs. (13) and (18), respectively. Thus, in the model of the α-FEM, the scaling factor α acts as a knob controlling the contributions from the NS-FEM and the FEM. When the factor α varies from 0 to 1, a continuous solution function from the solution of FEM to that of the NS-FEM is obtained.

4 Numerical error in acoustic problems

In the solution of the acoustic problems, the well-known issue of using numerical method including FEM is to control the numerical error. There is a so called "the rule of thumb" which requires a certain number of elements per wavelength to obtain a stabilized solution to the Helmholtz equation. However, the criterion is not reliable even if the rule of thumb is followed. In the following computations, the numerical discretization error in the H^1 semi-norm is used:

$$\left|p^e - p^h\right|_1^2 = \int_\Omega \left(\tilde{v}^e - \tilde{v}^h\right)^{\mathrm{T}} \left(v^e - v^h\right) \mathrm{d}\Omega \tag{26}$$

where $\tilde{v}$ is complex conjugate of the velocity v, the superscript e denotes the exact solutions and h denotes the numerical solutions obtained from numerical methods including the present α-FEM and FEM. Ihlenburg et al. showed that the relative error in the H^1 semi-norm can be estimated for a uniform hp-mesh of finite element method and it is bounded by [28]:

$$\eta = \frac{\left|p^e - p^h\right|_1}{|p|_1} \leq C_1' \left(\frac{kh}{p}\right)^p + C_2' k \left(\frac{kh}{p}\right)^{2p} \tag{27}$$

where C_1' and C_2' are constant independent of the parameters k and h, and p here is the degree of polynomial approximation used in the numerical methods. The relative error contains two terms: the first term is interpolation error which defines the difference between the interpolation and the exact solution; the second term is generally known as pollution error which defines the difference between the interpolation exact wave and the numerical solution of acoustic. For linear interpolation, it is shown in Ref. [29] that if $kh < 1$, the relative error for acoustic problems can be expressed by:

$$\eta \leq C_1 kh + C_2 k^3 h^2 \tag{28}$$

4.1 The dispersion error for FEM, NS-FEM and α-FEM in 1D problems

Consider an acoustic problem defined in a 1D domain Ω= (0, 1) with a Dirichlet boundary condition at the left end and a Robin boundary condition at the other end, which can be stated as follows.

$$\frac{d^2 p}{dx^2} + k^2 p = 0 \quad \text{in } \Omega\,(0 \leq x \leq 1) \tag{29}$$

$$p\,(0) = 1, \quad \left.\frac{dp}{dx}\right|_1 = -jkp(1) \tag{30}$$

This 1D problem has an analytical solution as follows:

$$p\,(x) = \cos\,(kx) + j\,\sin\,(kx) \tag{31}$$

The density of fluid is $1.225\,\mathrm{kg/m^3}$ and the velocity of the acoustic wave is 340 m/s. k is the non-dimensional wave number depending on the given frequency. Assuming that the 1D problem is discretized by a uniform mesh of $n(= 1/h)$ linear elements, the discrete equation corresponding to the node at x_i for FEM can be easily written as [30]:

$$Rp_{i-1} + 2Sp_i + Rp_{i+1} = 0 \tag{32}$$

where p_i is the nodal pressure value at node i, and the coefficients $R(\gamma)$ and $S(\gamma)$ are expressed as follows.

$$S = 1 - \frac{1}{3}\gamma^2, \quad R = -1 - \frac{1}{6}\gamma^2, \quad \gamma = kh \tag{33}$$

By substituting $p_i = e^{ik^{FEM}x_i}$ into Eq. (32), using the fact that the nodes $i-1$ and $i+1$ are the two neighbor nodes with $x_{i-1} = x_i - h$ and $x_{i+1} = x_i + h$, then the discrete wave number for standard FEM can be obtained as

$$\begin{aligned} k^{FEM} &= k - \frac{1}{24}k^3h^2 + O\left(k^5h^4\right) \\ &= k\left(1 - \frac{1}{24}k^2h^2 + O\left(k^4h^4\right)\right) \end{aligned} \tag{34}$$

As shown in Eq. (34), the wave number of FEM is smaller than the exact wave number, which leads to a shift phase in FEM solution.

We now derive the wave number expression for the NS-FEM. After assembling the global equation and multiplying the whole set of equations by h, we arrive at the following set of linear equations for the NS-FEM.

$$\mathbf{L}_h\mathbf{P} = \mathbf{F} \tag{35}$$

where the discrete operator $\mathbf{L}_h$ can be written as

$$\mathbf{L}_h = \begin{bmatrix} \tilde{S}+\frac{1}{2} & 2\tilde{R} & \tilde{R} & & & & \\ 2\tilde{R} & 2\tilde{S}+\frac{1}{4} & 0 & \tilde{R} & & & \\ \tilde{R} & 0 & 2\tilde{S} & 0 & \tilde{R} & & \\ & & \ddots & & & & \\ & \tilde{R} & 0 & 2\tilde{S} & 0 & \tilde{R} & \\ & & \tilde{R} & 0 & 2\tilde{S}+\frac{1}{4} & 2\tilde{R} & \\ & & & \tilde{R} & 2\tilde{R} & \tilde{S}+\frac{1}{2}+ik \end{bmatrix} \tag{36}$$

in which

$$\tilde{S} = \frac{1}{4} - \frac{1}{2}\gamma^2, \quad \tilde{R} = -\frac{1}{4}, \quad \gamma = kh \tag{37}$$

The discrete equation corresponding to node i can be rewritten as follows

$$\tilde{R}p_{i-2} + 2\tilde{S}p_i + \tilde{R}p_{i+2} = 0 \tag{38}$$

Using $x_{i-2} = x_i - 2h$ and $x_{i+2} = x_i + 2h$ and $p_i = e^{ik^{NS-FEM}x}$ (k^{NS-FEM} here is the wave number of NS-FEM yet to be determined), Eq. (38) becomes

$$\tilde{R}(\gamma)e^{ik^{\mathrm{NS-FEM}}(x_i-2h)} + 2\tilde{S}(\gamma)e^{ik^{\mathrm{NS-FEM}}x_i} + \tilde{R}(\gamma)e^{ik^{\mathrm{NS-FEM}}(x_i+2h)} = 0 \tag{39}$$

where

$$\lambda = e^{i2k^{\mathrm{NS-FEM}}h} \tag{40}$$

Eq. (39) can be solved for λ with

$$\lambda_{1,2} = (1-2\gamma^2) \pm \frac{\sqrt{(2-4\gamma)^2-4}}{2} = \begin{cases} \text{complex conjugate} & \text{if } \gamma < 1 \\ \text{real} & \text{if } \gamma > 1 \end{cases} \tag{41}$$

For case of $\gamma < 1$, the NS-FEM has a complex conjugate solution, and the discrete wave number of NS-FEM can be obtained by combining Eqs. (40)–(41):

$$\cos\left(2k^{\mathrm{NS-FEM}}h\right) = 1 - 2\gamma^2 \tag{42}$$

In this case, we arrived at

$$k^{\mathrm{NS-FEM}} = \frac{1}{2h}\arccos\left(1-2\gamma^2\right) \tag{43}$$

Using Taylor expansion

$$\arccos\left(1-2\gamma^2\right) = 2kh + \frac{1}{3}(kh)^3 + \frac{3}{20}(kh)^5 + O(kh)^5 \tag{44}$$

The wave number for NS-FEM can be expressed as following:

$$k^{\mathrm{NS-FEM}} = k\left(1 + \frac{1}{6}k^2h^2 + \frac{3}{40}k^4h^4 + O\left(k^4h^4\right)\right) \tag{45}$$

Equation (45) shows that the wave number of NS-FEM is always larger than the exact one, which is in complementary to the standard FEM. This important feature is rooted at the softening effects and upper bound solutions discovered in [21]: the FEM and NS-FEM solutions stays at the opposite sides of the exact solution.

The wave numbers of NS-FEM and FEM are also verified numerically using a mesh with nodal spacing of 0.05 for the frequency of 680 Hz, and the results are presented in Fig. 3. As shown in the figure, the wavelength of FEM is longer than the exact solution showing a phase-lagging behind the exact solution; while the wavelength of NS-FEM is shorter than the exact one showing a phase-leading ahead of the exact solution. This verifies numerically that the wave numbers

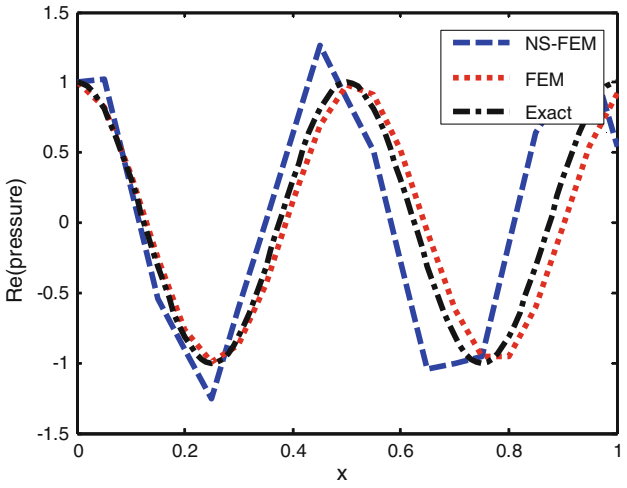

Fig. 3 Spatial distribution of real part of the pressure at 680 Hz obtained using NS-FEM and FEM with the same uniform mesh of nodal spacing of 0.05

of NS-FEM and FEM bound the exact wave number. This phenomenon is essential caused by the "overly-stiff" nature of the FEM model and "overly-soft" nature of the NS-FEM model. It is naturally expected that a properly formulated α-FEM model which combines the FEM and NS-FEM can provide a proper stiffness to the system minimizing the dispersion error.

To show the effectiveness of the α-FEM, this 1D problem is again investigated using both FEM and α-FEM at the frequency of 680 Hz. A uniform mesh with nodal spacing of 0.1 m (kh=1.26) is adopted. The results obtained from the FEM and the α-FEM ($\alpha = 0.1, 0.3$) are presented in Fig. 4. It is shown that the wavelength of FEM is also longer than the exact solution exhibiting obvious dispersion error; while the wavelength of α-FEM ($\alpha = 0.3$) is shorter than the exact. We found that the wavelength of α-FEM ($\alpha = 0.1$) matches closely the exact wave with the error mostly caused by the linear interpolation. Note these two values of α are chosen arbitrarily from the region of $a \in [0, 1]$.

4.2 The dispersion error for FEM, NS-FEM and α-FEM in 2D problems

For two dimensional problems, a "sequel regular" mesh with nodal spacing of h is considered as shown in Fig. 5, where the nodes contributing the FEM linear equation associated to node $S_{(i,j)}$ are marked. Using this type of mesh, a linear system similar as Eq. (35) can be obtained when solving the Helmholtz equation using FEM and NS-FEM. Here L_s^{FEM} and L_s^{NS-FEM} represent a row of the system equation associated to node $S_{(i,j)}$ in the FEM and NS-FEM linear equation system, respectively.

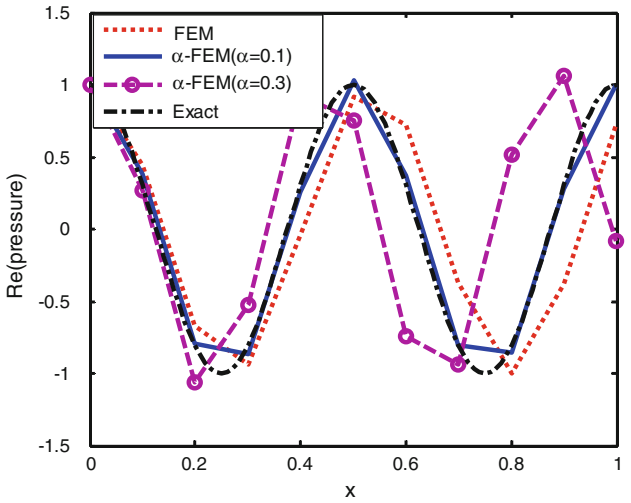

Fig. 4 Spatial distribution of real part of the pressure at 680 Hz with nodal spacing of 0.1 using α-FEM and FEM

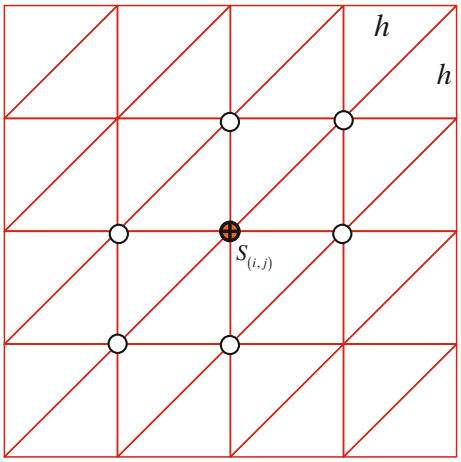

Fig. 5 The discretization near node (i, j) for both FEM and NS-FEM models

For the FEM model, the discrete equation corresponding to node $S_{(i,j)}$ can be written as follow:

$$L_s^{\mathrm{FEM}} = A_1 p_{i,j+1} + A_2 p_{i+1,j+1} + A_1 p_{i-1,j} + A_0 p_{i,j} + A_1 p_{i+1,j} + A_2 p_{i-1,j-1} + A_1 p_{i,j-1} = 0 \quad (46)$$

where

$$A_0 = 4 - \tfrac{1}{2}k^2h^2 \quad A_1 = -(1 + \tfrac{1}{12}k^2h^2) \quad A_2 = -\frac{1}{12}k^2h^2 \quad (47)$$

Note in two dimensions, the FEM solution of a plane wave has a form of

$$p(x) = Ae^{i(k_1x+k_2y)} \text{ with } k_1 = k^{\mathrm{FEM}}\cos\theta \quad k_2 = k^{\mathrm{FEM}}\sin\theta \quad (48)$$

Substituting Eq. (48) into Eq. (46), leads to

$$\begin{aligned} L_s^{\mathrm{FEM}}\left(k^{\mathrm{FEM}}\right) = {} & A_1 e^{i(k_1\cdot 0+k_2 h)} + A_2 e^{i(k_1 h+k_2 h)} \\ & + A_1 e^{i(k_1(-h)+k_2\cdot 0)} + A_0 e^{i(k_1\cdot 0+k_2\cdot 0)} \\ & + A_1 e^{i(k_1 h+k_2\cdot 0)} + A_2 e^{i(k_1(-h)+k_2(-h))} \\ & + A_1 e^{i(k_1\cdot 0+k_2(-h))} = 0 \end{aligned} \quad (49)$$

After simplification, we have

$$\begin{aligned} Re\left(L_s^{\mathrm{FEM}}\left(k^{\mathrm{FEM}}\right)\right) = {} & A_0 + 2A_1(\cos(k_1h) + \cos(k_2h)) \\ & + 2A_2\cos(k_1h + k_2h) = 0 \end{aligned} \quad (50)$$

For the NS-FEM model, we shall have

$$\begin{aligned} L_s^{\mathrm{NS-FEM}}\left(k^{\mathrm{NS-FEM}}\right) = {} & -B_3 p_{i,j+2} - B_1 p_{i+1,j+2} \\ & + B_1 p_{i+2,j+2} - B_2 p_{i-1,j+1} + B_1 p_{i,j+1} + B_2 p_{i+1,j+1} \\ & - B_1 p_{i+2,j+1} - B_3 p_{i-2,j} + B_1 p_{i-1,j} + B_0 p_{i,j} \\ & + B_1 p_{i+1,j} - B_3 p_{i+2,j} - B_1 p_{i-2,j-1} + B_2 p_{i-1,j-1} \\ & + B_1 p_{i,j-1} - B_2 p_{i+1,j-1} - B_1 p_{i-2,j-2} \\ & - B_1 p_{i-1,j-2} - B_3 p_{i,j-2} = 0 \end{aligned} \quad (51)$$

The plane wave of NS-FEM in a 2D domain shall have the following form:

$$p(x) = Ae^{i\left(k_1'x+k_2'y\right)} \quad \text{with} \quad k_1' = k^{\mathrm{NS-FEM}}\cos\theta \quad k_2' = k^{\mathrm{NS-FEM}}\sin\theta \quad (52)$$

Using similar approach, Eq. (51) becomes:

$$\begin{aligned} Re\left(L_s^{\mathrm{NS-FEM}}\left(k^{\mathrm{NS-FEM}}\right)\right) = {} & B_0 \\ & + 2B_1\left(\cos(k_1'h) + \cos(k_2'h) - \cos(k_1'h + 2k_2'h)\right. \\ & \left. - \cos(2k_1'h + k_2'h) - \cos(2k_1'h + 2k_2'h)\right) \\ & - 4B_2\sin(k_1'h)\sin(k_2'h) - 2B_3(\cos(2k_2'h) \\ & + \cos(2k_1'h)) = 0 \end{aligned} \quad (53)$$

It is clear that Eqs. (50) and (53) are not the equation for circles that are the exact solution for the plane wave in 2D space, which indicates that the FEM and NS-FEM always have some direction-dependent dispersion. Using polar coordinates, it is possible to plot the curve in the $(k_1, k_2)/(k_1', k_2')$ plane representing the numerical solution of wave number using both FEM and NS-FEM models. Figure 6 shows an example of kh=1, with h=1. In this figure, it is found that the dispersion is very large for the wave propagation direction between the $0^o \sim 90^o$ and $180^o \sim 270^o$, and relative small between the direction of the $90^o \sim 180^o$ and $270^o \sim 360^o$. This is true for both FEM and NS-FEM models. It is also observed that the wave number solution of FEM is always smaller than the exact solution, while the NS-FEM solution is larger than the exact one, in all wave propagation directions. Using alpha = 0.4, the solution of α-FEM can be tuned

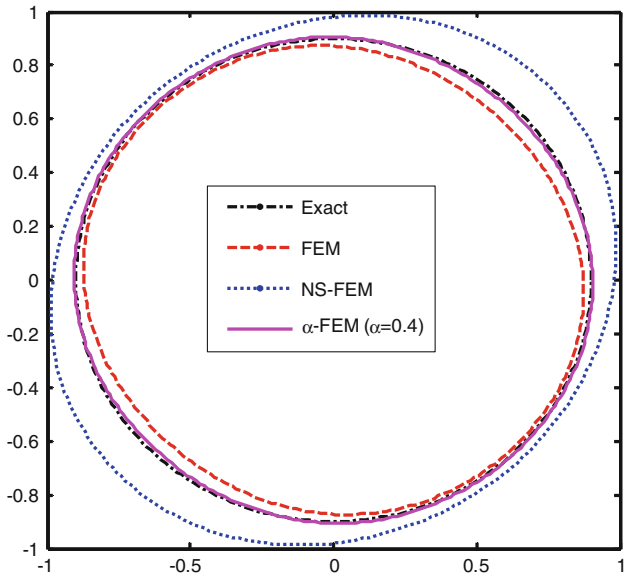

Fig. 6 Direction dependence of the exact (circle of radius $k=1$), FEM, NS-FEM, and α-FEM ($\alpha = 0.4$) solutions to the same Helmholtz equation. All the numerical solutions depend on the angle of acoustic wave propagation

locating in between the solutions of FEM and NS-FEM, and much closer to the exact solution, compared to both FEM and NS-FEM. Note the selection of alpha in the α-FEM is very critical in minimizing the dispersion error. Therefore, the determination of the parameter alpha will be discussed in more detail in the next section.

5 Determination of alpha

5.1 The determination of alpha in 1D problems

In this section, we present a general procedure to determine the important parameter alpha, which controls the contribution proportions of the FEM and NS-FEM to the present α-FEM model.

For 1D problem, the discrete equation of α-FEM in matrix L_h corresponding to node i can be given as

$$\begin{aligned}&\alpha\tilde{R}(\gamma)p_{i-2}+(1-\alpha)R(\gamma)p_{i-1}+2(1-\alpha)S(\gamma)p_i\\&\quad+2\alpha\tilde{S}(\gamma)p_i+(1-\alpha)R(\gamma)p_{i+1}\\&\quad+\alpha\tilde{R}(\gamma)p_{i+2}=0\end{aligned}\tag{54}$$

Using the similar procedure discussed in Sect. 4.1, Eq. (54) becomes:

$$\begin{aligned}&-\alpha\cos^2\left(k^{\alpha-\mathrm{FEM}}h\right)+2(1-\alpha)\left(-1-\frac{1}{6}\gamma^2\right)\cos(k^{\alpha-\mathrm{FEM}}h)\\&\quad+\left(2-\alpha-\frac{1}{3}\alpha\gamma^2-\frac{2}{3}\gamma^2\right)=0\end{aligned}\tag{55}$$

which is a nonlinear equation of α in relation to $k^{\alpha-FEM}$ that is the wave number of the α-FEM model. If an alpha can be found such that $k^{\alpha-FEM}$ equals to the exact k, we shall obtain a good α-FEM model with no dispersion error. This requirement is met by replacing the $k^{\alpha-FEM}$ with the exact k in Eq. (55), with this design criteria, the α can be determined:

$$\alpha=\frac{\left(2+(1/3)\gamma^2\right)\cos(\gamma)-2+(2/3)\gamma^2}{-\cos^2(\gamma)+2\cos(\gamma)+(1/3)\gamma^2\cos(\gamma)-(1/3)\gamma^2-1}\tag{56}$$

Using the parameter α determined by Eq. (56), the α-FEM can eliminate the dispersion error in the 1D acoustic problems, and the numerical error is only due to the interpolation error.

5.2 Determination of alpha in 2D problems

For two-dimensional problems discussed in Sect. 4.2, the discrete equation of α-FEM for nodes i can be expressed as follows:

$$\begin{aligned}&(1-\alpha)Re\left(L_s^{FEM}\left(k^{\alpha-FEM}\right)\right)\\&\quad+\alpha Re\left(L_s^{NS-FEM}\left(k^{\alpha-FEM}\right)\right)=0\end{aligned}\tag{57}$$

Based on the previous analysis, the optimal α can also be determined by replacing the $k^{\alpha-FEM}$ with the exact k in Eq (57):

$$\alpha=\frac{Re\left(L_s^{FEM}(k)\right)}{Re\left(L_s^{FEM}(k)\right)-Re\left(L_s^{NS-FEM}(k)\right)}\tag{58}$$

For a given value of direction of wave propagation θ, we can always obtain an α in Eq. (58) which can eliminate the dispersion error. The optimal α with relation to the wave propagation θ for different wave number and mesh size have been plotted in Fig. 7. It is shown in the figure that (i) the alpha varies with the wave propagation θ, while the changing trend of the alpha against the wave propagation angle is roughly the same; (ii) with the increase of wave number, the value of the alpha will increase accordingly.

Using Eq. (58) and the parameters $kh = 2$, $(h = 1)$, the optimal α with respect to each angle θ can be determined. We then plot the dispersion error for α-FEM with these optimal values of α in Fig. 8, together with the FEM using both triangular (T3) and quadrilateral (Q4) elements. It can be seen clearly that the α-FEM results are in a very good agreement with the analytical one. Relatively, the FEM results have very large dispersion error for both the linear (T3) and the bilinear (Q4) models.

It can also be drawn in the figures that the optimal alpha depends on the wave number, mesh size and the wave propagation angle in 2D problems, while this result is not very

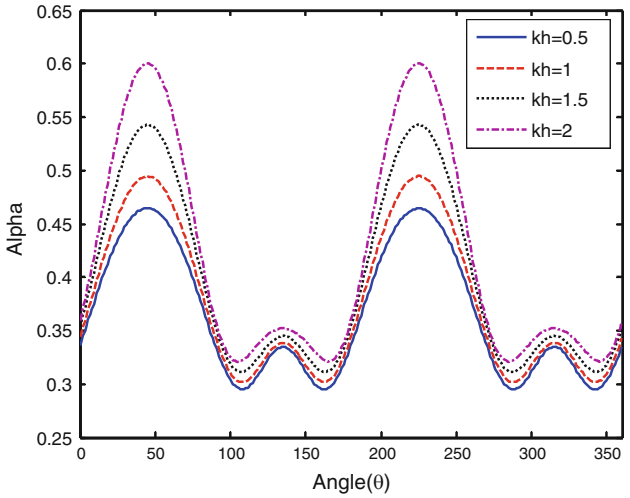

Fig. 7 The value of alpha varies with the wave propagation angle for different wave number and mesh size

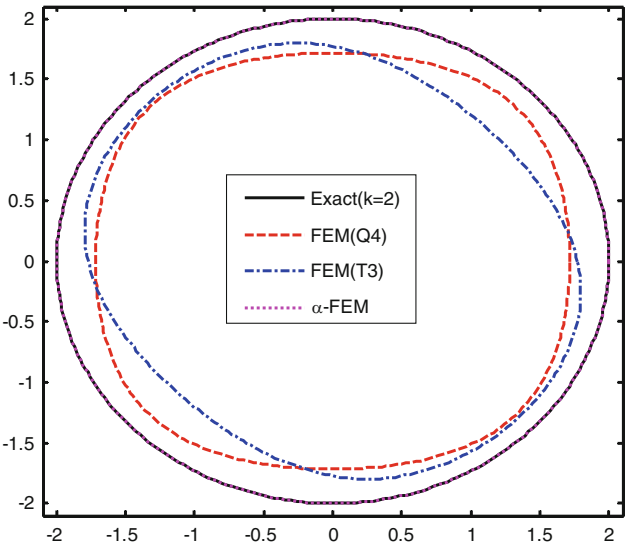

Fig. 8 Direction dependence of the exact (circle of radius $k=2$, with $h=1$), FEM, and α-FEM solutions to the same Helmholtz equation

useful in practice since the exact solution is never a single plane wave (but a sum of waves traveling in different directions). In this case, we need to select the optimal α based on the wave propagating angle with aim to reduce the maximum dispersion error. We can select the alpha numerically for Eq. (58), i.e. looping the wave propagation angle from 0° to 360° with small steps, for example, 0.001. As the values of alpha for different wave numbers have the same changing trend, we can find the optimal alpha at the specified wave propagation angle and thus minimize the maximum dispersion error from 0° to 360° for all wave number and mesh size. The optimal angle has been studied with $kh=1$,(h=1) and the results are plotted in Fig. 9. From the figure, the wave propagation angle which determines the

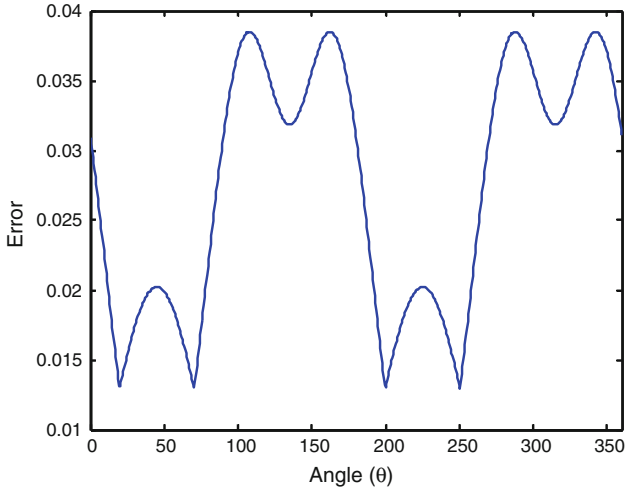

Fig. 9 The maximum dispersion error with related to the alpha for the specified wave propagation angle

optimal alpha can be obtained. Note that any other triangular mesh can be mapped to the present sequel regular mesh and the proof is similar as the quadrilateral mesh in [5]. So the present procedure to determine the optimal alpha is very general.

6 Numerical example

In this paper, two examples with analytical solutions and a real problem about the vehicle passenger compartment are studied in detail to investigate the accuracy and convergence of the α-FEM.

6.1 1D problem with Dirichlet boundary condition

Consider a wave propagating in the domain $\Omega=(0, 1)$ with Dirichlet boundary conditions described as follows:

$$\frac{d^2p}{d\xi^2}+k^2p=0 \quad \text{in } \Omega\,(0\le\xi\le 1) \tag{59}$$

$$p\,(0)=1, \quad \frac{dp}{d\xi}\,(1)=0 \tag{60}$$

The problem has an analytical solution as follows:

$$p\,(\xi)=\cos\,(k\xi)+\tan k\,\sin\,(k\xi) \tag{61}$$

The problem has eigenmodes corresponding to the values:

$$k=\left(n+\frac{1}{2}\right)\pi, \quad n\in N \tag{62}$$

Note that in the vicinity of the above values, the problem becomes numerically ill-posed which significantly increases the numerical error.

6.1.1 Acoustic error and convergence study

The density of fluid is 1.225 kg/m^3 and the velocity of the wave is 340 m/s. Three different frequency values (750 Hz ($k = 13.86$), 1,500 Hz ($k = 27.72$), 2,000 Hz ($k = 36.96$)) have been employed to study the problem using α-FEM with the nodal spacing of 0.05. In the α-FEM model, alpha calculated using Eq. (56) for different values of kh is employed. For the purpose of comparison, FEM solutions are also computed using the same mesh as well as in the α-FEM. The numerical results of acoustic pressure using α-FEM and FEM at different frequency values, together with the exact solutions, are plotted in Fig. 10. It can be seen from these plots that: for lower frequency value 750 Hz ($k = 13.86$, $kh < 1$), the α-FEM can provide very close-to-exact solution which is much more accurate than the FEM; for higher frequency values including 1500 and 2,000 Hz ($k = 27.72, 36.96$, $kh > 1$), the α-FEM also provides very good results and the error is mostly the approximation error, while FEM solutions depart a lot from the exact one.

The convergence and accuracy properties of α-FEM are then studied using four models with different numbers of uniformly distributed nodes (21, 41, 81, 161 nodes, respectively). Three frequency values 750 Hz ($k = 13.86$), 1,500 Hz ($k = 27.72$) and 2,000 Hz ($k = 36.96$) have been selected. The results obtained from the α-FEM and FEM in terms of global error are plotted together in Fig. 11. From this figure it can be found that the α-FEM obtains much better accuracy and higher convergence rate than the FEM; this is due to the dispersion free and very "close-to-exact" stiffness feature of the α-FEM.

6.1.2 Influence of the eigenfrequencies

The problem has analytical solution of eigenvalues corresponding to the wave number $k = (n + 1/2)\pi, n \in N$, for which the response and the global error are infinity. Due to the dispersion error, the numerical wave numbers of FEM are tending to different from the exact wave number with the increase of the frequency. In this section, the global error against wave number will be investigated using the present α-FEM and FEM. Figure 12 plots the global error as a function of wave number k with nodal spacing of 0.1 m. As shown in the figure, global error tends to infinity where the numerical wave numbers are close to the exact eigenvalues. With the increase of wave number, the FEM can not give the eigenvalues prediction observed with higher eigenvalues prediction or spurious eigenvalues, due to the dispersion of the numerical wave; while the α-FEM can provide very accurate eigenvalues prediction even when $kh > 1$, which is known as "the rule of thumb". This is because the gradient smoothing operation has been conducted in the α-FEM which can partially soften the structure and provide the "right-stiffness" to the acoustic model.

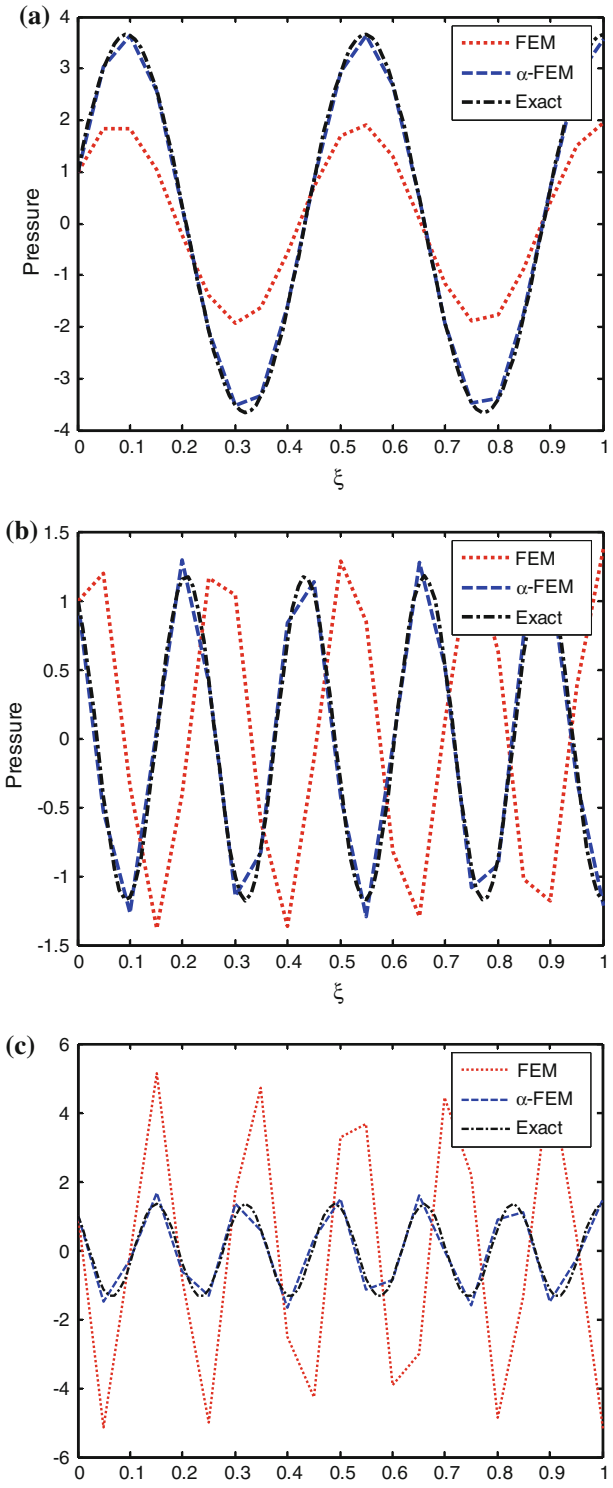

Fig. 10 Exact and numerical solutions of acoustic pressure at different frequency values for the 1D time-harmonic problem. **a** 750 Hz ($k = 13.86$, $kh = 0.693$), **b** 1,500 Hz ($k = 27.72$, $kh = 1.386$), **c** 2,000 Hz ($k = 36.96$, $kh = 1.848$)

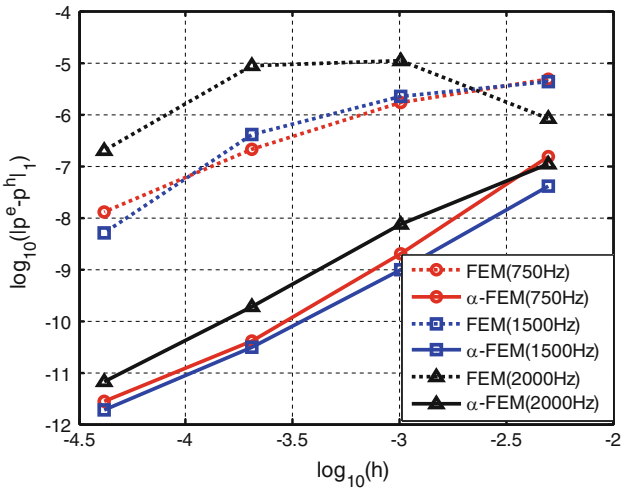

Fig. 11 Comparison of accuracy and convergence at different frequency values between the α-FEM and FEM for 1D problem

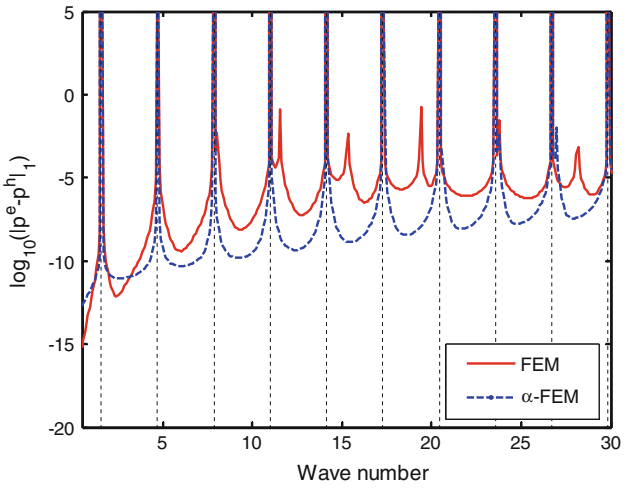

Fig. 12 The global error for different nodal spacing $h = 0.1$

6.2 2D Problem with Neumann boundary condition

Another problem for interior acoustic simulations is a 2D rectangular tube filled with air as shown in Fig. 13. The dimension of this tube with length l=1 m and width b=0.24 m is considered. The left of the tube is subjected to normal velocity boundary condition with v_n=0.01 m/s, the right end of the tube is rigid wall and the normal velocity v=0 m/s. The density of air ρ is 1.225 kg/m^3 and the speed of sound in the air is 340 m/s. The analytical solutions for this problem can be easily derived and the pressure and velocity are given by

$$p = -j\rho c v_n \frac{\cos(k(1-\xi))}{\sin(k)} \tag{63}$$

$$v = \frac{v_n \sin(k(1-\xi))}{\sin(k)} \tag{64}$$

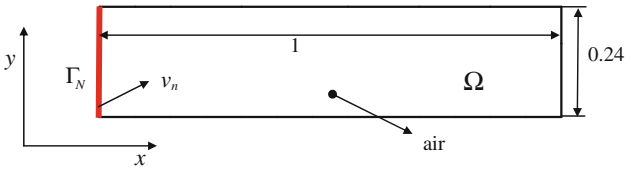

Fig. 13 2D acoustic chamber with the Neumann boundary condition

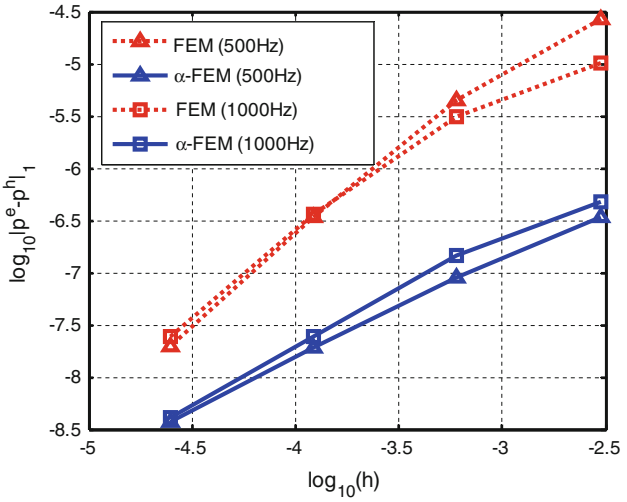

Fig. 14 Comparison of accuracy and convergence at different frequency values between the α-FEM and FEM for 2D problem

The problem also has eigenmodes corresponding to the values:

$$k = 2\pi n \tag{65}$$

6.2.1 Convergence study

The convergence property is investigated by employing four models with 58, 186, 669 and 2,541 uniformly distributed nodes with nodal spacing of 0.08, 0.04, 0.02 and 0.01 m. Figure 14 presents the convergence curves in terms of global error against the average nodal spacing h at frequency of 500 and 1,000 Hz for both α-FEM and FEM simulations. From these figures, it can be observed that the present α-FEM can give much more accurate results than that of FEM.

6.2.2 Influence of the eigenfrequencies

The problem also has analytical solution of eigenvalues corresponding to the wave number $k = 2\pi n, n \in N$. In this section, the global error against wave number will also be investigated using the present α-FEM and FEM. Figure 15 plots the global error as a function of wave number with nodal spacing of 0.08 and 0.04 m. The results shown in the figure also demonstrate the similar conclusions above that

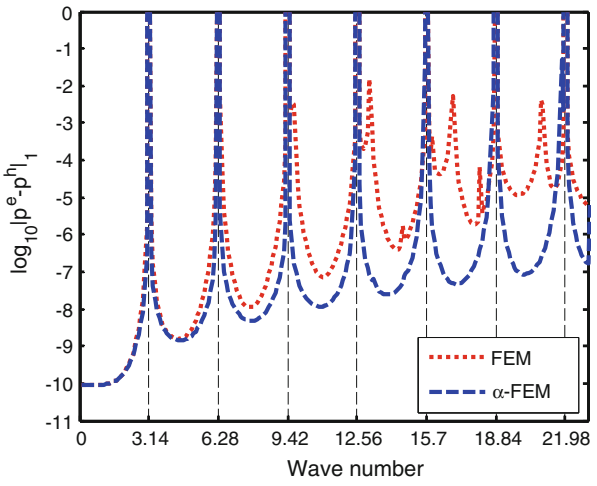

Fig. 15 The global error for different nodal spacing

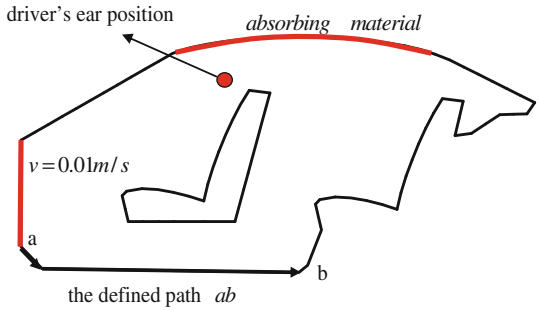

Fig. 16 Acoustic problem for a 2D car with different boundary conditions, the results on $\overrightarrow{ab}$ path will be closely examined

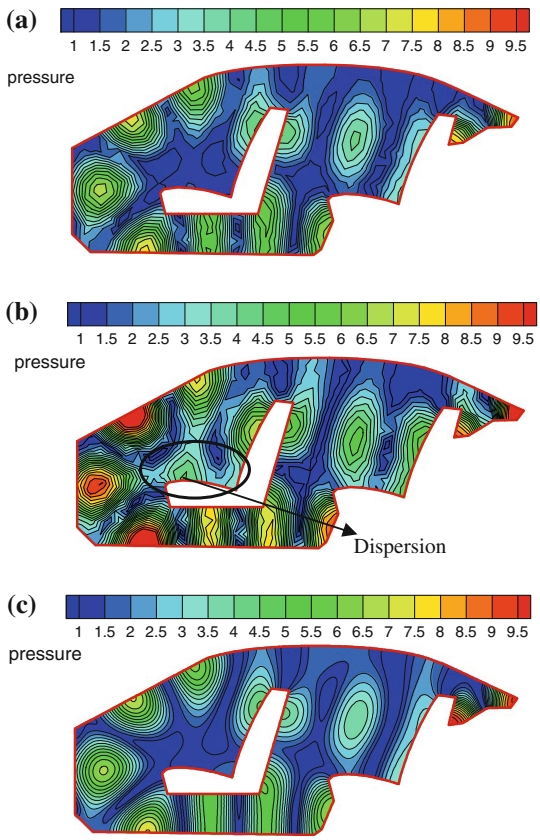

Fig. 17 **a** Acoustic pressure distribution obtained using α-FEM (500 Hz). **b** Acoustic pressure distribution obtained using FEM (500 Hz). **c** Acoustic pressure distribution obtained using Reference (500 Hz)

(i) with the increase of wave number, the FEM gives higher eigenvalues or spurious eigenvalues prediction (ii) while the α-FEM can also provide very accurate eigenvalues solution even $kh > 1$, which far beyond the "the rule of thumb". This also verifies the "right-stiffness" of the α-FEM for 2D acoustic problems.

6.3 2D car acoustic problem

Acoustic pressure distribution in a car passenger compartment, which has been frequently used as a benchmark in acoustic simulation, is also adopted to study the efficiency of α-FEM. Figure 16 illustrates the 2D geometry of the problem domain. The maximum size of this domain is $L_x = 2.664$m in the horizontal and $L_y = 1.121$m in the vertical. The acoustical fluid is air and the parameter is the same as the previous. As one of the main sources generating the noise in the passenger compartment is engine vibration. The front panel of the passenger compartment is subjected to the vibration coming from the engine with the velocity of 0.01 m/s. The roof of the passenger compartment is fixed with absorbing material with admittance of $0.00144\text{m}^3/(\text{Pa}\cdot\text{s})$.

This domain is dicretized with 361 nodes with nodal spacing of 0.08 m, which gives a frequency limit of 676 Hz by the "the rule of thumb". The frequency values of 500 Hz ($kh = 0.74$) and 650 Hz ($kh = 0.96$) will be investigated using the α-FEM in this model. Figures 17a and 18a show

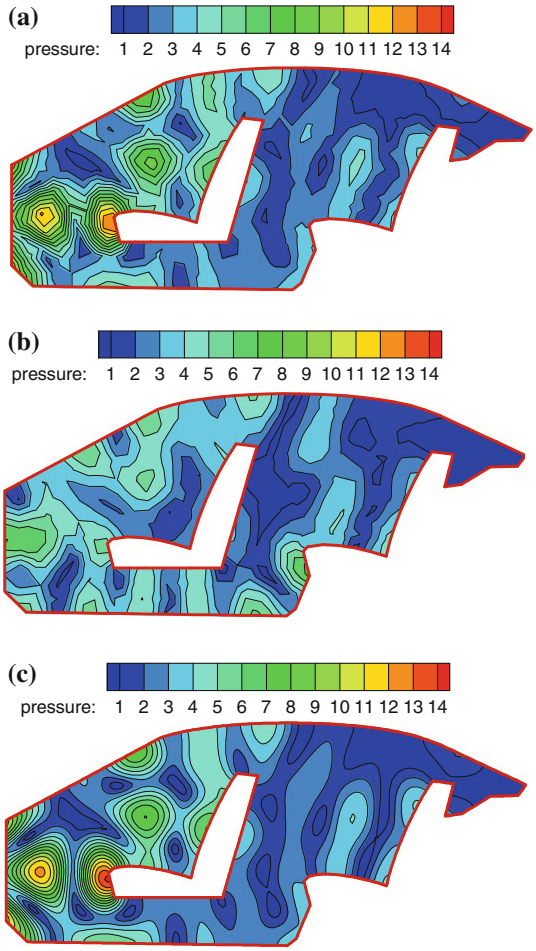

Fig. 18 **a** Acoustic pressure distribution obtained using α-FEM (650 Hz). **b** Acoustic pressure distribution obtained using FEM (650 Hz). **c** Acoustic pressure distribution obtained using Reference (650 Hz)

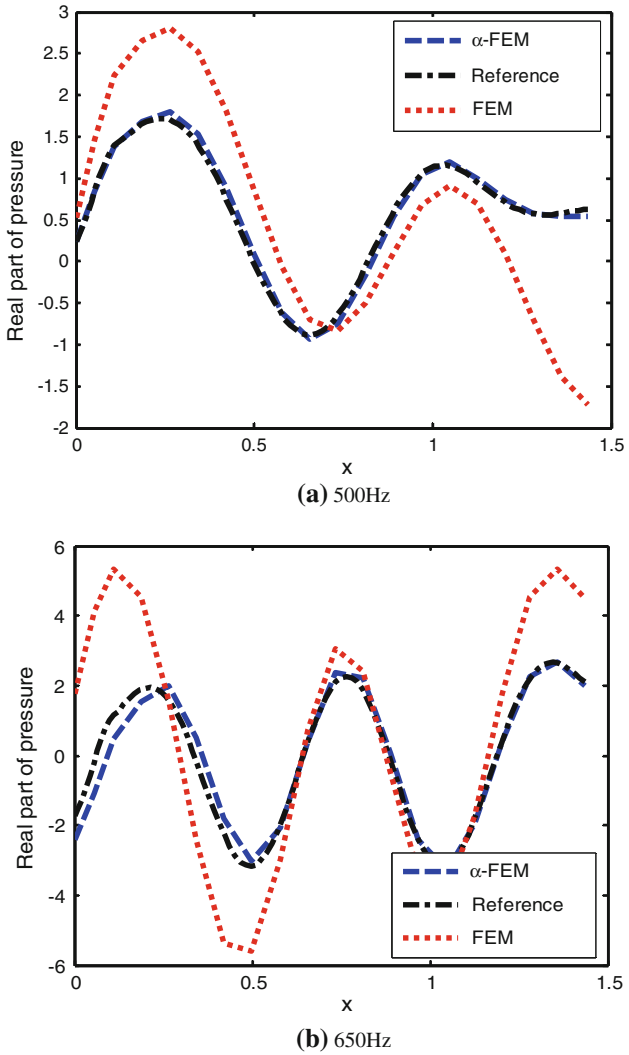

Fig. 19 Real part of acoustic pressure distribution along the path $\overrightarrow{ab}$ at different frequency values

the distribution of acoustic pressure in the passenger compartment at 500 and 650 Hz obtained from the α-FEM, while the results obtained using the FEM at 500 and 650 Hz are plotted in Figs. 17b and 18b, respectively. Because the analytical solution is unavailable for this problem, a reference configuration using FEM with a very fine mesh (8,951 nodes) is adopted and the results at 500 and 650 Hz are plotted in Figs. 17c and 18c.

From these figures, it can be observed that the FEM solution shows the dispersion error around the seat at 500 Hz. When it comes to higher frequency value ($f = 650$ Hz), the FEM error is obvious due to the dispersion, as most of the contours of the acoustic pressure are departing from the reference solution. While the α-FEM can provide similar contours to the references at both the frequency values of 500 and 650 Hz, and showed only little dispersion. To show the results quantitatively, the real part of pressure obtained from the α-FEM and FEM along the defined path $\overrightarrow{ab}$ shown in Fig. 16 at different frequency values are given in Fig. 19a and b, respectively. The solution of FEM along the defined path $\overrightarrow{ab}$ shows the dispersion and deviates from the reference solution a lot; while the α-FEM solution exhibits better than that of the FEM. We found even for the frequency of 650 Hz, the real part of acoustic pressure obtained from the α-FEM along the defined path $\overrightarrow{ab}$ varies a little from the reference result. This again demonstrates the α-FEM is much more accurate than FEM.

Then the direct frequency response analysis is also conducted using present α-FEM and FEM with previous Neumann and Admittance boundary conditions. A full range frequency sweep is done from 1 to 1,000 Hz at intervals of 1.0 Hz which is beyond the frequency value limit 676 Hz, and the response (sound pressure level) at the driver's ear point, which is illustrated in Fig. 16, is measured. The results using α-FEM and FEM are depicted in Fig. 20. As the analytical solution is unavailable, a reference solution using FEM

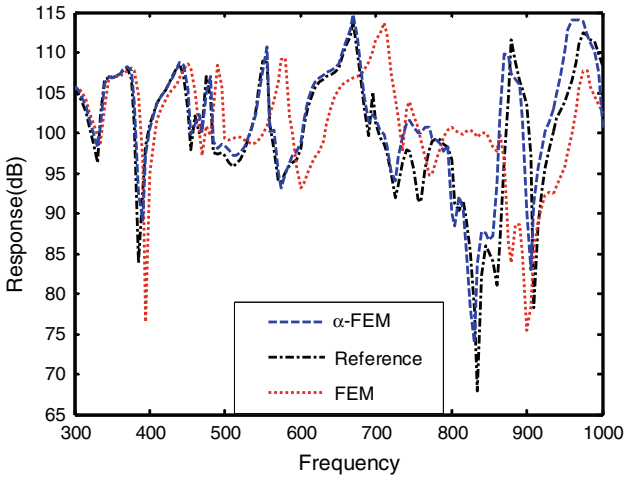

Fig. 20 Acoustic frequency response at driver's ear point for 2D car problem using α-FEM and FEM

with 8951 nodes is also provided. As shown in the figure, the α-FEM can provide much better result than FEM in the full frequency range even the frequency exceeds 676 Hz; while error of FEM solution can be obviously observed for higher frequency value. This numerical example validates that α-FEM possesses an appropriately softened effect compared with the "overly-stiff" FEM model and can give more accurate solution even at high frequencies.

7 Conclusions and discussions

In this work, the alpha finite element method (α-FEM) is formulated for solving 1D and 2D acoustic problems. In the α-FEM, a combined model is obtained by a scaled factor $\alpha \in [0,1]$, making the best use of the "overly-stiff" FEM model and the "overly-soft" node-based finite element method (NS-FEM) model. A general way to find out the optimal value of alpha has been presented for both 1D and 2D problems and a number of numerical examples have been studied. The following conclusions can be derived:

a) The wave number of the NS-FEM is larger than the exact one, which is in complementary to the standard FEM whose wave number is smaller than the exact.
b) The α-FEM has the same dimension with the FEM model by using same mesh and the method can be implemented in a straightforward way with little change to the FEM code.
c) The parameter α introduced in the α-FEM model controls the ratio of the contributions from the FEM and the NS-FEM models. The procedure to determine the optimal α is very general and can be easily performed.
d) Owing to the optimal alpha and gradient smoothing operation used in the model, the α-FEM processes an appropriately softened effect and close-to-exact stiffness dramatically reducing the dispersion error. Numerical studies also demonstrate that the present α-FEM can achieve higher accuracy than the FEM especially for higher wave number, and provide much better eigenfrequencies prediction in acoustic analysis.

Finally, we note that for acoustics problems governed by the Helmholtz equations, the most effective approach to improve the accuracy of the numerical solution is not through the increase of the density of the mesh, but via a smart tuning of the numerical model as we have done in our α-FEM.

Acknowledgments The author wish to thank the support of the China-funded Postgraduates' Studying Aboard Program for Building Top University and the National Natural Science Foundation of China. This work is partially supported by A*Star, Singapore. It is also partially supported by the Open Research Fund Program of the State Key Laboratory of Advanced Technology of Design and Manufacturing for Vehicle Body, Hunan University, People's Republic of China under the grant number 40915001.

References

1. Harari I, Magoulès F (2004) Numerical investigations of stabilized finite element computations for acoustics. Wave Motion 39:339–349
2. Babuška I, Ihlenburg F, Paik ET, Sauter SA (1995) A generalized finite element method for solving the Helmholtz equation in two dimensions with minimal pollution. Comp Methods Appl Mech Eng 128:325–359
3. Harari I, Hughes TJR (1992) Galerkin/least squares finite element methods for the reduced wave equation with non-reflecting boundary conditions in unbounded domains. Comp Methods Appl Mech Eng 98:411–454
4. Thompson LL, Pinsky PM (1995) A Galerkin least squares finite element method for the two-dimensional Helmholtz equation. Int J Numer Methods Eng 38(3):371–397
5. Deraemaeker A, Babuska I, Bouillard Ph (1999) Dispersion and pollution of the FEM solution for the Helmholtz equation in one, two and three dimension. Int J Numer Methods Eng 46:471–499
6. Petersen S, Dreyer D, Estorff Ov (2006) Assessment of finite and spectral element shape functions or efficient iterative simulations of interior acoustics. Comp Methods Appl Mech Eng 195:6463–6478
7. Biermann J, Estorff Ov, Petersen S, Wenterodt C (2009) Higher order finite and infinite elements for the solution of Helmholtz problems. Comput Meth Appl Mech Eng 198:1171–1188
8. Babuška I, Melenk JM (1997) The partition of unity method. Int J Numer Methods Eng 40:727–758
9. Babuška I, Melenk JM (1996) The partition of unity finite element method: basic theory and applications. Comp Methods Appl Mech Eng 139:289–314
10. Alvarez GB, Loula AFD, Dutra do Carmo EG, Rochinha FA (2006) A discontinuous finite element formulation for Helmholtz eqation. Comp Methods Appl Mech Eng 195:4018–4035
11. Loula AFD, Alvarez GB, Dutrado Carmo EG, Rochinha FA (2007) A discontinuous finite element method at element level for Helmholtz equation. Comp Methods Appl Mech Eng 196:867–878

12. Bouillard Ph, Suleau S (1998) Element-free Garlekin solutions for Helmholtz problems: formulation and numerical assessment of the pollution effect. Comp Methods Appl Mech Eng 162:317–335
13. Suleau S, Deraemaeker A, Bouillard Ph (2000) Dispersion and pollution of meshless solution for the Helmholtz equation. Comp Methods Appl Mech Eng 190:639–657
14. He ZC, Liu GR, Zhong ZH, Wu SC, Zhang GY, Cheng AG (2009) An edge-based smoothed finite element method (ES-FEM) for analyzing three-dimensional acoustic problems. Comp Methods Appl Mech Eng 199:20–33
15. Liu GR, Nguyen TT (2010) Smoothed finite element methods. CRC Press, Boca Raton
16. Liu GR (2008) A generalized gradient smoothing technique and the Smoothed bilinear form for Galerkin formulation of wide class of computational methods. Int J Comput Methods 5:199–236
17. Liu GR (2009) Meshfree methods: moving beyond the finite element method, 2nd edn. CRC Press, Boca Raton
18. Liu GR, Zhang GY, Dai KY, Wang YY, Zhong ZH, Li GY, Han X (2005) A linearly conforming point interpolation method (LC-PIM) for 2D solid mechanics problems. Int J Comput Methods 2(4):645–665
19. Zhang GY, Liu GR, Wang YY, Huang HT, Zhong ZH, Li GY, Han X (2007) A linearly conforming point interpolation method (LC-PIM) for three-dimensional elasticity problems. Int J Numer Methods Eng 72(13):1524–1543
20. Liu GR, Nguyen TT, Nguyen XH, Lam KY (2009) A node-based smoothed finite element method for upper bound solution to solid problems. Comput Struct 87:14–26
21. Liu GR, Zhang GY (2008) Upper bound solution to elasticity problems: a unique property of the linearly comforming point interpolation method (LC-PIM). Int J Numer Methods Eng 74:1128–1161
22. Liu GR, Nguyen TT, Lam KY (2009) An edge-based smoothed finite element method (ES-FEM) for static, free and forced vibration analysis. J Sound Vib 320:1100–1130
23. Liu GR, Nguyen TT, Lam KY (2008) A novel alpha finite element method (aFEM) for exact solution to mechanics problems using triangular and tetrahedral elements. Comp Methods Appl Mech Eng 197:3883–3897
24. Liu GR, Zhang GY (2009) A normed G space and weakened weak (W^2) formulation of a cell-based smoothed point interpolation method. Int J Comput Methods 6(1):147–179
25. Liu GR (2010) A weakened weak (W2) form for a unified formulation of compatible and incompatible methods, part I: theory and part II: applications to solid mechanics problems. Int J Numer Methods Eng 81:1093–1156
26. Liu GR (2009) On a G space theory. Int J Comput Methods 6(2): 257–289
27. Liu GR, Zhang GY (2008) Edge-based smoothed point interpolation methods. Int J Comput Methods 5(4):621–646
28. Ihlenburg F, Babuška I (1997) Reliability of finite element methods for the numerical computation of waves. Adv Eng Softw 28:417–424
29. Irimie S, Bouillard Ph (2001) A residual a posteriori error estimator for the finite element solution of the Helmholtz equation. Comp Methods Appl Mech Eng 190:2027–2042
30. Ihlenburg F, Babuška I (1995) Finite element solution of the Helmholtz equation with high wave number part I: the *h*-version of the FEM. Comput Math Appl 30(9):9–37